Cell Reports
Methods

Report

Rapid detection of an Ebola biomarker with optical microring resonators

Graphical abstract

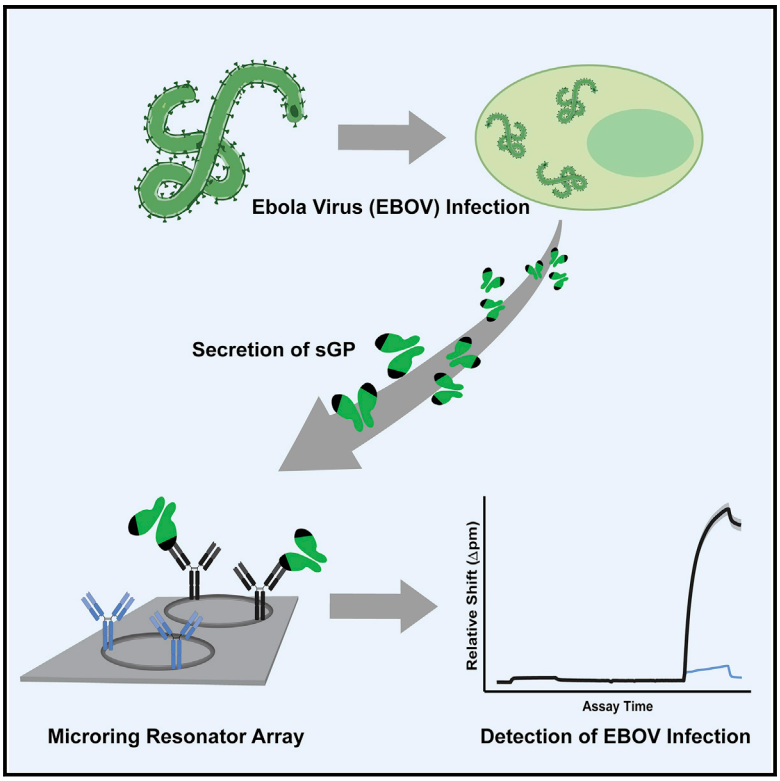

Authors

Abraham J. Qavi, Krista Meserve, M. Javad Aman, ..., Frederick W. Holtsberg, Ryan C. Bailey, Gaya K. Amarasinghe

Correspondence

rick@integratedbiotherapeutics.com (F.W.H.),
ryancb@umich.edu (R.C.B.),
gamarasinghe@wustl.edu (G.K.A.)

In brief

Qavi et al. describe a method using microring resonator sensors to detect Ebola virus (EBOV) soluble glycoprotein (sGP) in serum. sGP is a promising biomarker for the prognosis of EBOV infection and, coupled with this rapid detection method, could lead to a faster diagnosis.

Highlights

- sGP is a unique diagnostic marker of Ebola virus infection
- Microring resonators can detect EBOV and SUDV sGP at low ng/mL concentrations
- Our sandwich immunoassay design enables the detection of antigens from serum
- Multiplex chip has flexible design, technical replicates, and integrated controls

Qavi et al., 2022, Cell Reports Methods 2, 100234
June 20, 2022
https://doi.org/10.1016/j.crmeth.2022.100234

CellPress

Cell Reports Methods

CellPress
OPEN ACCESS

Report

Rapid detection of an Ebola biomarker with optical microring resonators

Abraham J. Qavi,[1,9] Krista Meserve,[2,9] M. Javad Aman,[3] Hong Vu,[3] Larry Zeitlin,[4] John M. Dye,[5] Jeffrey W. Froude,[6] Daisy W. Leung,[7] Lan Yang,[8] Frederick W. Holtsberg,[3,*] Ryan C. Bailey,[2,*] and Gaya K. Amarasinghe[1,10,*]

[1]Department of Pathology & Immunology, Washington University School of Medicine, St. Louis, MO 63110, USA
[2]Department of Chemistry, University of Michigan, Ann Arbor, MI 48109, USA
[3]Integrated Biotherapeutics, Rockville, MD 20850, USA
[4]Mapp Biopharmaceutical, Inc., San Diego, CA 92121, USA
[5]United States Army Medical Research Institute of Infectious Diseases, Fort Detrick, MD 21702, USA
[6]United States Army Nuclear and Countering Weapons of Mass Destruction Agency, Fort Belvoir, VA 22060, USA
[7]Department of Medicine, Washington University School of Medicine, St. Louis, MO 63110, USA
[8]Department of Electrical & Systems Engineering, Washington University in St. Louis, St. Louis, MO 63130, USA
[9]These authors contributed equally
[10]Lead contact
*Correspondence: rick@integratedbiotherapeutics.com (F.W.H.), ryancb@umich.edu (R.C.B.), gamarasinghe@wustl.edu (G.K.A.)
https://doi.org/10.1016/j.crmeth.2022.100234

MOTIVATION Filoviruses, such as Ebola virus, are highly infectious pathogens with high mortality rates. Current diagnostics for filoviruses mainly rely on PCR-based techniques, ELISAs, or lateral flow assays. Disadvantages of these techniques include limited multiplexing capabilities, limited quantitative information, and lengthy assay times. We present a method for the detection of Ebola virus that addresses these concerns, with a total assay time of under 40 min.

SUMMARY

Ebola virus (EBOV) is a highly infectious pathogen, with a case mortality rate as high as 89%. Rapid therapeutic treatments and supportive measures can drastically improve patient outcome; however, the symptoms of EBOV disease (EVD) lack specificity from other endemic diseases. Given the high mortality and significant symptom overlap, there is a critical need for sensitive, rapid diagnostics for EVD. Facile diagnosis of EVD remains a challenge. Here, we describe a rapid and sensitive diagnostic for EVD through microring resonator sensors in conjunction with a unique biomarker of EBOV infection, soluble glycoprotein (sGP). Microring resonator sensors detected sGP in under 40 min with a limit of detection (LOD) as low as 1.00 ng/mL in serum. Furthermore, we validated our assay with the detection of sGP in serum from EBOV-infected non-human primates. Our results demonstrate the utility of a high-sensitivity diagnostic platform for detection of sGP for diagnosis of EVD.

INTRODUCTION

RNA viruses are an area of critical concern and a major threat to global health; between 25% and 44% of all emerging infectious diseases are caused by RNA viruses (Binder et al., 1999; Jones et al., 2008; Morens et al., 2004; Woolhouse and Gowtage-Sequeria, 2005). This is in part attributed to their ability to mutate rapidly, a consequence of low-fidelity RNA-dependent RNA polymerases (Bishara et al., 2011; Greenbaum et al., 2013; Institute of Medicine Committee on emerging Microbial threats to Health et al., 1992; McLeod et al., 2014; Mudanyali et al., 2013), as well as increased contact between both humans and zoonotic vectors (Carrasco-Hernandez et al., 2017). Filoviruses are among the most lethal human single-stranded, negative-sense RNA viruses, with high case fatality rates up to 89% during outbreaks (Rugarabamu et al., 2020). Ebola virus (EBOV) is the causative agent of EBOV disease (EVD), characterized by pathognomonic symptoms of internal and external bleeding, in addition to a constellation of non-specific symptoms including fever, fatigue, nausea, vomiting, diarrhea, and headache (Beeching et al., 2014).

Previous outbreaks of EBOV highlight the need for rapid diagnostics to accurately and rapidly detect disease. Access to diagnostic information is critical for disease management by enabling healthcare systems to initiate isolation protocols and begin supportive measures that drastically improve patient outcomes (Chertow et al., 2014; Khan et al., 1999; Lindblade et al., 2015). In resource-limited settings, accurate diagnosis also enables

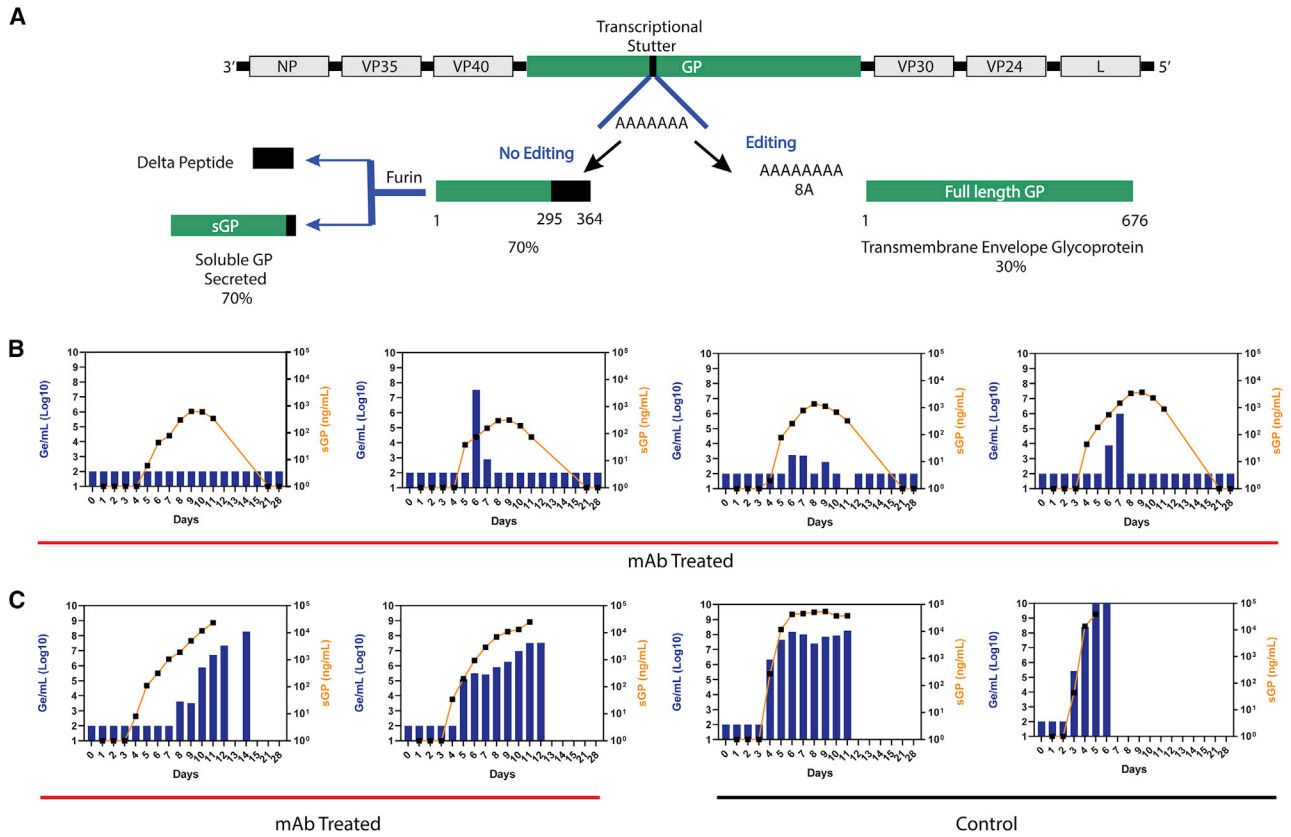

Figure 1. Ebola virus genome, generation of sGP, and comparison of EBOV RT-PCR versus sGP values during infection

(A) The Ebola genome contains seven genes, including one encoding for glycoprotein (GP). A transcriptional stutter leads to the addition of seven additional adenosines, which are edited to result in the full-length, transmembrane GP. In contrast, without editing, a soluble GP (sGP) is formed, which is secreted from the infected cell.

(B and C) Comparison of RT-PCR values (blue bars) and an ELISA for sGP (orange lines) in non-human primates (NHPs) infected with EBOV who (B) survived and (C) were deceased. Treatment either with monoclonal antibody (mAb) or control (no treatment) is reflected under the plots.

healthcare providers to utilize limited resources more efficiently to limit the outbreak spread. Current diagnostics for EBOV mainly rely on PCR-based techniques, ELISAs, or lateral flow assays with varying degrees of success (Broadhurst et al., 2016; Furuyama and Marzi, 2020; Kebenei and Okoth, 2021; Moran et al., 2020). Each of these methods require additional electronics for sample processing and trained technicians to perform studies. Moreover, these techniques have several disadvantages, including low multiplexing capabilities, limited quantitative information, lengthy assay times, and/or the requirement of centralized laboratories or cold chain custody. Specific to EVD, these assays rely on either the glycoprotein (GP) of EBOV or nucleic acid-based testing, both of which are subject to a diagnostic window period during which infected patients will test negative. Therefore, new technologies that bypass traditional analytical limitations and technical requirements as well as informative actional biomarkers of EVD are needed to enable effective triaging and treatment of infected individuals.

The EBOV genome, consisting of seven genes, is highlighted in Figure 1A. EBOV GP is expressed as two distinct transcriptional products. These two proteins are expressed through site-specific transcriptional editing of the GP gene. The primary product of the GP gene is the soluble GP (sGP), a nonstructural secreted GP that is expressed from the unedited RNA transcript. sGP is dimerized by two cysteine bridges and released from EBOV-infected cells (Pallesen et al., 2016; Volchkova et al., 1998). The full-length GP, which coats the surface of mature viral particles, is expressed only following transcriptional editing of the GP gene, where an additional uridine residue is added to the genomic RNA. This editing adds an additional adenosine residue in the transcript, which results in an extended open reading frame. The majority of transcripts are non-edited and therefore sGP is the first and predominant product of GP gene transcription and translation (Sanchez et al., 1998; Volchkova et al., 1998). sGP shares the first 295 residues with GP but contains a unique C-terminal tail.

There are several roles sGP appears to play in EBOV pathogenesis. It has been proposed that the expression and secretion of sGP allows EBOV to evade the host immune response via immune decoy leading to increased virulence (de La Vega et al., 2015; Zhu et al., 2019). Additionally, sGP has been shown to have immune modulatory functions. It inhibits pro-inflammatory cytokine production by macrophages, limits macrophage migration (Bradley et al., 2018), and reduces CD16b receptors on

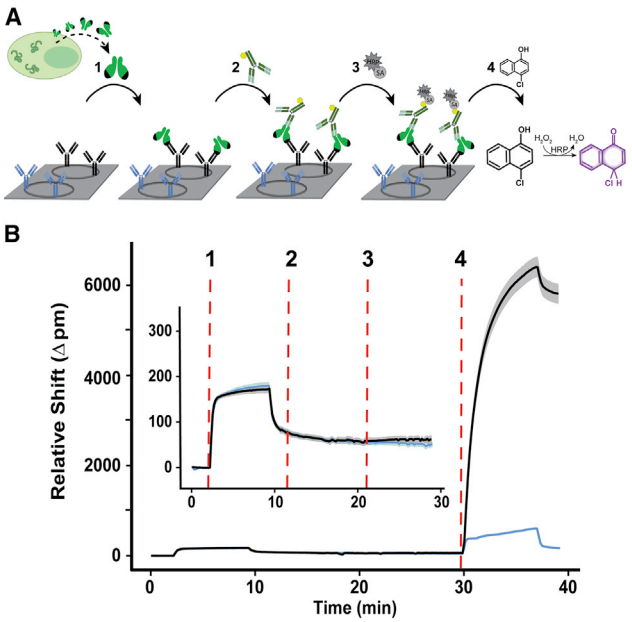

Figure 2. Schematic of sGP detection with microring resonators

(A) General workflow of sGP detection from infection to sample analysis. During infection, sGP is secreted from infected cells into the patient's circulation and is isolated in patient serum. The immunoassay begins by binding of the secreted sGP in serum (1) onto the functionalized microring surface using specific antibodies (black), while off-target antibodies serve as negative controls (blue). As a secondary recognition element, biotinylated pan-filoviral antibodies (2) detect the captured sGP. This sandwich complex is recognized by streptavidin horseradish peroxidase (3), which allows for enzymatic processing of solution-phase 4-chloro-1-napthol (4). This final step leads to a large shift in resonant wavelength that is proportional to the amount of sGP bound by the capture antibodies.

(B) Corresponding microring traces for each of the steps in (A). The solid line reflects the average response of 8–12 technical replicates, while the surrounding halo reflects the spread of individual rings. Inset reflects the steps 1–3.

human neutrophils (Kindzelskii et al., 2000). sGP has been reported to have a protective function in the context of endothelial layer integrity as well, which may support viral replication (Wahl-Jensen et al., 2005). sGP also activates the MAP kinase signaling pathway, which is thought to increase the uptake and internalization of EBOV virions (Furuyama and Marzi, 2020). Despite sGP's numerous functions, its role as a biomarker is only now being appreciated.

In this study, we address critical diagnostic gaps for EVD by adapting a silicon photon microring resonator platform to detect EBOV sGP. Microring resonators are a class of whispering gallery mode (WGM) device in which light circulating within the microring interacts with biomolecules deposited on the ring surface, resulting in a shift in the ring's resonant wavelength that is proportional to the amount of the surface-adsorbed material. WGM devices have been leveraged for sensing applications over the past decade due to their amenability to multiplexing, high analytical sensitivity, quick time to result, and ease of integration with microfluidics. This has enabled their use in a wide variety of applications, including the detection of nucleic acids (Qavi and Bailey, 2010; Qavi et al., 2011; Scheler et al., 2012), proteins (Kindt et al., 2013; Shia and Bailey, 2013; Washburn et al., 2009), and viruses (McClellan et al., 2012). Recent work has integrated this sensing platform into clinical workflows to use varying biomarkers to profile disease states for diagnostic use (Cardenosa-Rubio et al., 2019; Robison et al., 2019, 2021; Wade et al., 2015). We demonstrate that microring resonators are an effective sensing platform for the rapid, multiplexed detection of filoviral infection using sGP. We also establish sGP as a sentinel biomarker and potential prognostic marker of EVD outcome with anticipated benefits in outbreak management.

RESULTS

The EBOV genome consists of seven genes, with sGP resulting from an unedited transcription of the GP gene (Figure 1A). This secreted protein was detected using an ELISA assay developed by Integrated Biotherapeutics and compared with RT-PCR in non-human primates (NHPs) infected with EBOV (Figures 1B and 1C). Samples were obtained following infection with EBOV in both treated and untreated NHPs. In all cases, sGP levels increased earlier or at the same time as RT-PCR values. Furthermore, NHPs with EBOV levels greater than 1,000 ng/mL succumbed to disease regardless of treatment status. These results reinforce sGP as both a diagnostic and prognostic marker of EBOV infection.

We utilized a silicon photonic microring resonator platform for the detection of sGP. Microring resonators operate on the principle of WGM sensing and continue to be a promising layout for biosensing applications due to ease of fabrication, chip integration, and high multiplexing potential (Figure S1) (Jiang et al., 2020; Yu et al., 2021). Light at a specific resonant wavelength is confined in small microring cavities. As changes in the local refractive index (RI) in the sensing region occur, the resonant wavelength within the microcavity shifts, which can be tracked in near real time. As each biomolecular binding event occurs over the course of the sandwich-style immunoassay, the resonant wavelength shifts relative to the initial wavelength. The extent of the final net shift is proportional to the amount of analyte bound on the microring resonator.

We first sought to validate the sandwich immunoassay and assess antibody specificity. The steps of the developed immunoassay on the microring platform consist of sample introduction followed by secondary recognition and amplification steps, highlighted in Figure 2A. Antibodies for EBOV sGP and Sudan virus (SUDV) sGP were functionalized in a multiplex fashion on the surface of the microrings, with each capture agent spanning 8–12 microrings to provide technical replicates. The sample of interest was introduced to the sensor surface through microfluidic fittings and automated with pumps as previously described (Figure 2A, step 1) (Arnfinnsdottir et al., 2020; Medfisch et al., 2020; Mordan et al., 2020; Robison and Bailey, 2017; Robison et al., 2019; Wetzler et al., 2020). As the antigen is flowed across the surface of the sensor, the primary binding occurred as EBOV sGP was captured by the anti-EBOV sGP antibodies on the sensor surface. After addition of sample, a buffer rinse washed away unbound material prior to introduction of the recognition molecule, a pan-EBOV-SUDV biotinylated tracer antibody

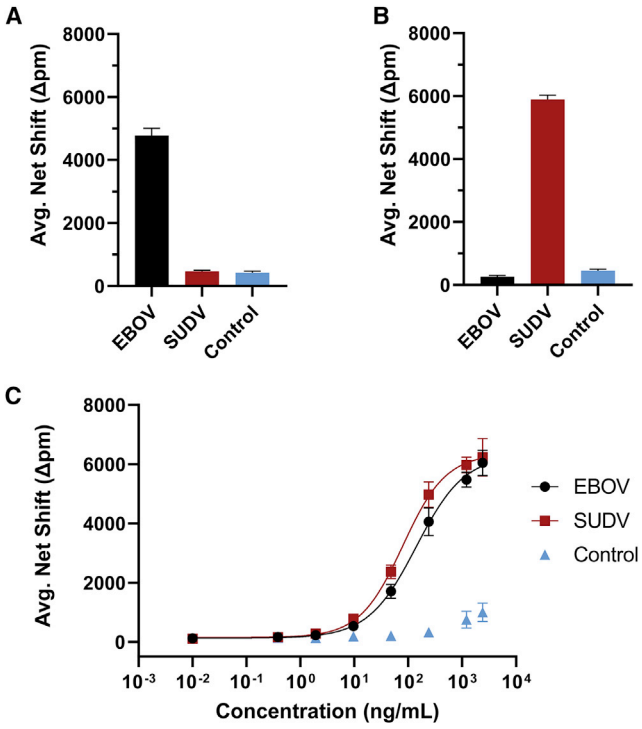

Figure 3. Cross-reactivity of microring resonators and calibration curves

Development of immunoassay for EBOV sGP and SUDV sGP detection. Chips functionalized with anti-EBOV sGP antibodies (black) and anti-SUDV sGP antibodies (red) show no cross-reactivity, as only those rings functionalized with the specific antibody elicit a response in the presence of the respective protein standard. Mouse IgG antibodies (blue) were functionalized on every chip as negative controls. Error bars represent n = 8–12 technical replicates.

(A) Sensor chip with 600 ng/mL of EBOV sGP.

(B) Sensor chip with 600 ng/mL SUDV sGP.

(C) Calibration curves of both targets detected simultaneously in 1% serum.

produced by Integrated Biotherapeutics (Figure 2A, step 2), to form a sandwich motif. This secondary tracer antibody recognizes multiple filovirus strains via conserved binding epitopes on the filoviral GP. These binding epitopes are different than those used with the primary antibody. Using a second antibody for this purpose increases the specificity of the assay, as any agent non-specifically adhered to the capture antibodies would not be recognized. After a buffer rinse, SA-HRP was flowed across the sensor surface (Figure 2A, step 3). In the final amplification step, 4-chloro-1-napthol (4CN) reacts with the HRP to form an insoluble product (Figure 2A, step 4). The precipitate is localized on the sensor surface, leading to a drastic change in refractive index proportional to EBOV sGP concentration. Unbound reagent is washed away with a final buffer rinse, and the net shift of resonant wavelength from the start of the 4CN amplification step to the end of the final buffer rinse is used for analysis. Incorporating these amplification steps leads to resonant wavelength shifts of ~6,000 pm for the highest concentrations, resulting in a larger dynamic range and lower limits of detection in comparison with using the primary antigen binding steps. An example trace of wavelength shift during the assay for detection of EBOV sGP with controls is highlighted in Figure 2B.

To address antibody specificity, cross-reactivity experiments were performed between EBOV and SUDV sGP. SUDV and EBOV are related species within the Ebolavirus genus, and SUDV also secretes sGP. The EBOV and SUDV sGPs were individually introduced to a sensor chip covalently functionalized with anti-EBOV sGP, anti-SUDV sGP, and mouse immunoglobulin (IgG) antibodies. Mouse IgG antibodies were used as negative controls to monitor non-specific adsorption interactions and resonant wavelength shifts due to bulk refractive index change. Only the sensor rings functionalized with the respective antibody responded to introduction of EBOV or SUDV sGPs (Figures 3A and 3B). When exposed to EBOV sGP, the anti-EBOV sGP functionalized rings (black) increase over the final amplification step, leading to a measurable net shift, while the anti-SUDV sGP functionalized rings (red) and control functionalized rings (blue) have low net shifts (<1,000 pm). The same trend is observed with an SUDV sGP target, where the anti-SUDV sGP functionalized rings result in a large net shift, while the anti-EBOV sGP and control functionalized rings have comparable shifts. There was no evidence of cross-reactivity in these assays, which is attributed to the specificity of the primary capture antibodies.

Calibration of EBOV and SUDV sGP occurred simultaneously over a range of concentrations spanning from undetectable levels to saturation of the signal (Figure 3C). The net shifts for all concentrations were fitted to a logistic function for calculation of unknown concentrations based on net shift,

$$y = \frac{A_1 - A_2}{1 + \left(\frac{x}{x_0}\right)^p} + A_2 \qquad \text{(Equation 1)}$$

where y is the net shift of the sample, A_1 is the maximum net shift (Δpm), A_2 is the minimum net shift (Δ pm), x is the sample analyte concentration (pM), x_0 is the center value (pM), and p is the power parameter affecting the slope around the inflection point (Table S1) (Robison and Bailey, 2017; Robison et al., 2021). The calibration curve (Figure 3C) was constructed in the biologic matrix of 1% serum. Curves were also constructed for 10% and 50% serum (Figure S3). The limit of detection (LOD) for EBOV sGP and SUDV sGP were determined to be 1.72 ng/mL and 1.00 ng/mL in 1% sera, respectively; 4.20 ng/mL and 1.54 ng/mL in 10% sera, respectively; and 2.33 ng/mL and 7.76 ng/mL in 50% sera, respectively (Table S2). We calculated the LOD as the concentration correlating to the sensor response three standard deviations from the blank signal. Our calibration curves of spiked sGP into pooled human sera demonstrated a decreased LOD with increased percentage of serum. However, given that the LOD from 1% serum to 50% serum decreased by ~2.5-fold for EBOV and ~5-fold for SUDV, we anticipated no difficulties in detecting sGP from the NHP samples.

Analysis of NHP samples were done at 10× or 100× dilutions due to limited sample volume. Each sample was analyzed using the same experimental and data extraction methods as the calibrations, with each sample taking just under 40 min to complete. The researchers were blinded to the subject number and outcome of subject but did know a relative range of concentrations

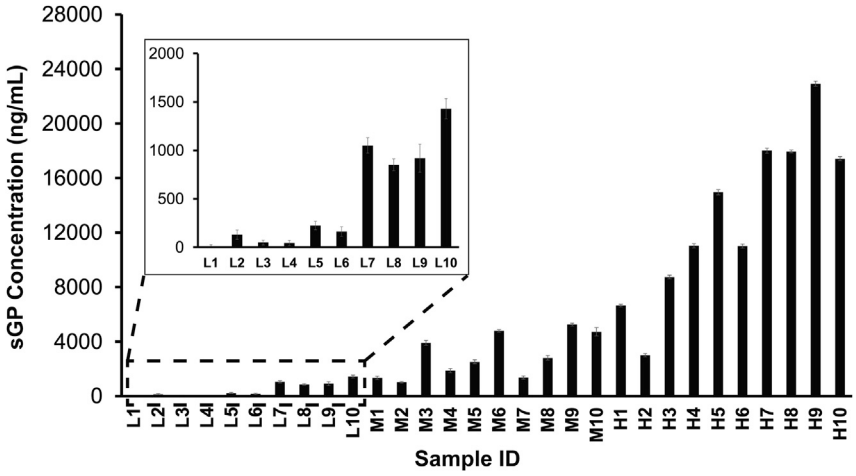

Figure 4. Detection of sGP from EBOV-infected NHP samples

Average net shift and SD of microring resonators toward EBOV-infected NHP samples. Error bars reflect ±1 SD. Samples designated with L refer to a sGP concentration range (confirmed via ELISA) between 100 and 1,000 ng/mL, M corresponding to 1,000–10,000 ng/mL, and H corresponding to 10,000–60,000 ng/mL. A total of 8–12 technical replicates were performed for each sample.

of EBOV sGP in each sample to make appropriate dilutions for this preliminary work. For the samples analyzed at two dilutions, the dilution that resulted in the net shift closest to the calibration curve inflection point was used for concentration determination. The 10× dilution was the most generalizable, ultimately being used for 24 of the 30 samples (Figure 4). The remaining six samples were those of highest sGP concentrations, resulting in the 10× dilution falling in the saturating range of the calibrations. However, the 100× dilution resulted in quantifiable results for these remaining. Additionally, only one of the 30 samples contained sGP below the LOD. Comparison of the microring resonators and ELISA assay are highlighted in Figure S4 and Table S3. The microring platform had a positive correlation with the ELISAs (R^2 = 0.94), but error rates of the microring platform relative to ELISA varied between 2.5% and 88.7%.

DISCUSSION

The ongoing COVID-19 pandemic highlights the need for sensitive diagnostic platforms and novel biomarkers. EBOV sGP represents a unique and powerful biomarker for the detection of EBOV infection and EVD prognosis for several reasons. The presence of sGP in the blood prior to, or simultaneously with, PCR-based assays improves the diagnostic window. As previously noted, survival outcomes from EBOV infection depend critically on the initiation of supportive measures, which heavily rely on accurate diagnoses in resource-limited settings. Rapid diagnosis facilitates faster treatment initiation, thereby improving patient outcomes (Chertow et al., 2014; Feldmann and Geisbert, 2011; Fowler et al., 2014). Quarantine of affected individuals has profound implications in infection and outbreak management and prevention. Alternatively, a confirmation of a negative test allows for healthcare providers to efficiently leverage their resources in treating patients. Because sGP is a protein biomarker, there is flexibility in the assay designs that can be used with the biomarker (e.g., lateral flow assays). The NHP study suggests that levels higher than 1,000 ng/mL of sGP may be a potential prognostic marker of EVD. Further studies are necessary to fully characterize the prognostic value of sGP.

The role of sGP as a diagnostic marker for infection has been previously explored by several groups. In one instance, researchers leveraged a modified D4 assay in combination with scFv-Fc antibodies generated from phage-display libraries for the highly sensitive detection of EBOV sGP (Fontes et al., 2021). Similar to our study, Fontes et al., confirmed the presence of sGP in EBOV-infected NHP with both a D4 assay and by RT-PCR. A critical difference is the use of fluorescence-based measurements, which requires a hand-held fluorescence reader. The D4 assay platform provides highly sensitive, multiplexed measurements; however, scalability of manufacturing may be challenging. In contrast, Wang and coworkers demonstrated the use of nanoparticles functionalized with nanobodies against EBOV sGP with a turn-around-time (TAT) of as little as 5 min (Chen et al., 2022). Through aggregation of nanoparticles and optimization of nanobody pairs, the researchers were able to detect both EBOV sGP and the receptor binding domain (RBD) of GP using a low-cost LED reader. The authors of this study only went up to 5% pooled sera and whole blood, due to the significant decrease in LOD seen due to matrix effects.

Initial development of the EBOV sGP assay using the microring resonators focused on the direct, label-free binding of sGP to the capture antibodies (Figures S2A and S2B). Label-free detection of analytes has been demonstrated in the past with microring resonators (Qavi and Bailey, 2010; Scheler et al., 2012; Washburn et al., 2009); however, the LOD has typically remained in the low ng/mL level for proteins in neat, buffered solutions. Our results were consistent with these findings, as no reliable calibration curve could be constructed based on primary binding data in a neat-running buffer at low ng/mL concentrations. Even more challenging is the elimination of primary binding profiles due to bulk RI shift upon the addition of a complex matrix (e.g., serum). Given that the prognostic value of sGP rests around 1,000 ng/mL, and that direct detection of antigens in sera is significantly more difficult due to matrix effects, label-free detection was insufficient for our purposes. We subsequently employed a two-step sandwich assay with an amplification step (Kindt et al., 2013). While the tracer antibody binding and amplification steps result in additional assay time, they provides drastically increased sensitivity and working dynamic range (Figures S2C and S2D). Furthermore, because signal amplification is performed in neat, buffered solutions in a separate step from sample

introduction, there are no interfering matrix effects that would be seen with direct binding in sera or plasma (Connell, 2012). An added benefit of the assay format is the use of a pan-Ebola monoclonal antibody (mAb) as a tracer antibody; that is, a single tracer antibody can be employed despite multiple primary capture antibodies and targets, simplifying the workflow of the assay.

An advantage of our sensor platform is the multiplexed capabilities, with 128 active sensors per chip. While our study highlights three targets on a single chip, the microring resonator platform has demonstrated up to 13-plex measurements on a single chip (Robison et al., 2021). The total multiplexing of targets is limited in part by the spotting of the capture antibodies on chip, as well as the number of desired technical replicates per run. Nonetheless, the current assay design can be adapted toward a broad range of pathogens. Given the non-specific symptoms seen with EVD that overlap significantly with other endemic tropical diseases (e.g., malaria), there is potential to further improve the capabilities of this assay by including additional targets (de Wit et al., 2016). Another advantage is addition of unfunctionalized thermal control microrings, which negates any environmental fluxes that may influence measurements. Additionally, our covalent linkage chemistry utilizes BS3, a homobifunctional crosslinker that reacts agnostically with primary amines. This ability to use unmodified antibodies or other capture agents and swap components within the assay represents a significant benefit in flexibility of assay design.

One concern with the microring assay is the percentage error from ELISAs. Despite higher analytical sensitivity compared with the ELISAs, our results suggested variable error in sGP concentration from the ELISA samples (Figure S4). At higher concentrations, the error appears to approach ~60%. It is unclear whether this is due to degradation of the sample over time, as the NHP samples were originally obtained in 2013, or a fundamental limitation of mass diffusion of the antigens. The microring platform leverages active fluidics in comparison with ELISAs relying on incubation steps. Further studies are necessary to resolve this discrepancy. Nonetheless, our platform was able to successfully detect EBOV sGP in 29 out of the 30 NHP samples. With the limited NHP samples available, we had to dilute samples to reach the minimum volume of ~300 μL to run the assay. Given the assay's ability to calibrate in 50% serum with limited decrease in the LOD, we anticipate no significant problems in the direct analysis of serum.

Another concern of the microring resonator platform is the expense of the instrument for an in-field assay. While the single-use disposable chips and cartridges are cost effective, the optical readout system itself can be cost-prohibitive, especially in resource-limited settings. There have been pushes to reduce the cost of these systems, either through distributed Bragg reflect (DRB) lasers (Xu et al., 2016) or alternate tuning mechanisms (Adolphson et al., 2022). Additionally, this instrument is not portable but is well suited for a field hospital or laboratory.

An additional concern with the assay is biocontainment. While the need for biocontainment is a consideration for any assay running human samples, this is especially relevant in the context of biosafety level 4 (BSL-4) work. One potential solution is pretreatment of samples for EBOV inactivation. Current methods include the use of irradiation (Elliott et al., 1982; Sagripanti and Lytle, 2011), alkylating agents (Warfield et al., 2007), acetic acid with heat (Mitchell and McCormick, 1984), or Triton X-100 with heat (Lau et al., 2015). An alternative to inactivation would be a self-contained sensor unit. In the context of WGM sensors, optofluidic devices such as liquid core optical ring resonators (LCORRs) (Suter et al., 2008; Zhu et al., 2007) or microbubble resonators (Giannetti et al., 2015) integrate the optical sensor component with fluidic handling.

Together, our results indicate that microring resonators that detect sGP are an appealing diagnostic platform for the detection of EBOV infection. We demonstrate that sGP is a diagnostic and prognostic marker for EBOV infection and, when leveraged in conjunction with a sensitive diagnostic assay, can provide actionable clinical information. Our work provides proof of concept and a framework for further optimization and assay development. Multiplexed measurements enabled by our platform will allow for a broader range of pathogens to be assessed, as well as the potential to incorporate other biomarkers relevant toward infection.

Limitations of the study

While our study highlights a potential biomarker for EVD and a new utility of the sensor platform, there are some areas for future development. Our technique requires the use of an instrument capable of interrogating optical resonators, which requires a tunable laser source within an optical readout instrument. While there have been pushes to miniaturize these instruments (Xu et al., 2016), current devices are laboratory based and one of the most expensive components of the assay. *De novo* detection of these antigens is not possible with our assay format. Further work is also required to fully characterize the diagnostic and prognostic value of sGP in EVD.

STAR★METHODS

Detailed methods are provided in the online version of this paper and include the following:

- KEY RESOURCES TABLE
- RESOURCE AVAILABILITY
  - Lead contact
  - Materials availability
  - Data and code availability
- METHOD DETAILS
  - Capture agents and antigens
  - Photonic microring resonators
  - Chemical functionalization and immobilization of capture antibodies on sensor chips
  - Assay set-up
  - Calibrations and sample analysis
  - NHP sera samples
  - ELISAs
  - PCR
- QUANTIFICATION AND STATISTICAL ANALYSIS
  - Microring resonator data analysis

SUPPLEMENTAL INFORMATION

Supplemental information can be found online at https://doi.org/10.1016/j.crmeth.2022.100234.

ACKNOWLEDGMENTS

A.J.Q. was funded by the T32 Cancer Biology Award (NIH CA009547). Opinions, interpretations, conclusions, and recommendations are those of the authors and are not necessarily endorsed by the US Army. This work was supported in part by NIH grants P01AI120943 and R01AI123926 to G.K.A., R41AI152745 to G.K.A. and F.W.H., R01AI141591 to R.C.B., and R01AI107056 to D.W.L. A.J.Q. acknowledges the support of the Department of Pathology and Immunology PSTP program and mentoring from Drs. Cote, French, Gronowski, Lenschow, and Payton.

AUTHOR CONTRIBUTIONS

A.J.Q., M.J.A., K.M., F.W.H., D.W.L., L.Y., R.C.B., and G.K.A. conceived this study. NHP studies were performed by M.J.A., H.V., L.Z., J.M.D., J.W.F., and F.W.H. Microring studies were performed by A.J.Q. and K.M. Data analysis was performed by A.J.Q., K.M., R.C.B., and G.K.A. Initial manuscript draft was written by A.J.Q. and K.M. and edited by G.K.A. and D.W.L. with input from all authors.

DECLARATION OF INTERESTS

R.C.B. has minor financial interest in Genalyte, Inc. M.J.A., H.V., and F.W.H. are employees of Integrated BioTherapeutics, Inc. L.Z. is co-owner of Mapp Biopharmaceutical, Inc.

Received: March 2, 2022
Revised: April 28, 2022
Accepted: May 16, 2022
Published: June 8, 2022

REFERENCES

Adolphson, M., Qavi, A., Shmuylovich, L., Amarasinghe, G.K., and Yang, L. (2022). Reverse tuning of whispering gallery mode microresonators. In Optics and Biophotonics in Low-Resource Settings VIII, *11950* (SPIE), pp. 10–15.

Arnfinnsdottir, N.B., Chapman, C.A., Bailey, R.C., Aksnes, A., and Stokke, B.T. (2020). Impact of silanization parameters and antibody immobilization strategy on binding capacity of photonic ring resonators. Sensors *20*, 3163. https://doi.org/10.3390/s20113163.

Beeching, N.J., Fenech, M., and Houlihan, C.F. (2014). Ebola virus disease. BMJ *349*, g7348. https://doi.org/10.1136/bmj.g7348.

Binder, S., Levitt, A.M., Sacks, J.J., and Hughes, J.M. (1999). Emerging infectious diseases: public health issues for the 21st century. Science *284*, 1311–1313. https://doi.org/10.1126/science.284.5418.1311.

Bishara, W., Sikora, U., Mudanyali, O., Su, T.-W., Yaglidere, O., Luckhart, S., and Ozcan, A. (2011). Holographic pixel super-resolution in portable lensless on-chip microscopy using a fiber-optic array. Lab Chip *11*, 1276–1279. https://doi.org/10.1039/c0lc00684j.

Bradley, J.H., Harrison, A., Corey, A., Gentry, N., and Gregg, R.K. (2018). Ebola virus secreted glycoprotein decreases the anti-viral immunity of macrophages in early inflammatory responses. Cell Immunol. *324*, 24–32. https://doi.org/10.1016/j.cellimm.2017.11.009.

Broadhurst, M.J., Brooks, T.J.G., and Pollock, N.R. (2016). Diagnosis of ebola virus disease: past, present, and future. Clin. Microbiol. Rev. *29*, 773–793. https://doi.org/10.1128/cmr.00003-16.

Cardenosa-Rubio, M.C., Robison, H.M., and Bailey, R.C. (2019). Recent advances in environmental and clinical analysis using microring resonator-based sensors. Curr. Opin. Environ. Sci. Health *10*, 38–46. https://doi.org/10.1016/j.coesh.2019.09.001.

Carrasco-Hernandez, R., Jácome, R., López Vidal, Y., and Ponce de León, S. (2017). Are RNA viruses candidate agents for the next global pandemic? A review. ILAR J. *58*, 343–358. https://doi.org/10.1093/ilar/ilx026.

Chen, X., Kang, S., Ikbal, M.A., Zhao, Z., Pan, Y., Zuo, J., Gu, L., and Wang, C. (2022). Synthetic nanobody-functionalized nanoparticles for accelerated development of rapid, accessible detection of viral antigens. Biosens. Bioelectron. *202*, 113971. https://doi.org/10.1016/j.bios.2022.113971.

Chertow, D.S., Kleine, C., Edwards, J.K., Scaini, R., Giuliani, R., and Sprecher, A. (2014). Ebola virus disease in west africa — clinical manifestations and management. N. Engl. J. Med. *371*, 2054–2057. https://doi.org/10.1056/nejmp1413084.

Connell, E. (2012). Tietz textbook of clinical chemistry and molecular diagnostics (5th edn). Ann. Clin. Biochem. *49*, 615. https://doi.org/10.1258/acb.2012.201217.

de La Vega, M.-A., Wong, G., Kobinger, G.P., and Qiu, X. (2015). The multiple roles of sGP in Ebola pathogenesis. Viral Immunol. *28*, 3–9. https://doi.org/10.1089/vim.2014.0068.

de Wit, E., Falzarano, D., Onyango, C., Rosenke, K., Marzi, A., Ochieng, M., Juma, B., Fischer, R.J., Prescott, J.B., Safronetz, D., et al. (2016). The merits of malaria diagnostics during an ebola virus disease outbreak. Emerg. Infect. Dis. *22*, 323–326. https://doi.org/10.3201/eid2202.151656.

Elliott, L.H., McCormick, J.B., and Johnson, K.M. (1982). Inactivation of lassa, marburg, and ebola viruses by gamma irradiation. J. Clin. Microbiol. *16*, 704–708. https://doi.org/10.1128/jcm.16.4.704-708.1982.

Feldmann, H., and Geisbert, T.W. (2011). Ebola haemorrhagic fever. Lancet *377*, 849–862. https://doi.org/10.1016/s0140-6736(10)60667-8.

Fontes, C.M., Lipes, B.D., Liu, J., Agans, K.N., Yan, A., Shi, P., Cruz, D.F., Kelly, G., Luginbuhl, K.M., Joh, D.Y., et al. (2021). Ultrasensitive point-of-care immunoassay for secreted glycoprotein detects Ebola infection earlier than PCR. Sci. Transl. Med. *13*. https://doi.org/10.1126/scitranslmed.abd9696.

Fowler, R.A., Fletcher, T., Fischer, W.A., Lamontagne, F., Jacob, S., Brett-Major, D., Lawler, J.V., Jacquerioz, F.A., Houlihan, C., O'Dempsey, T., et al. (2014). Caring for critically ill patients with ebola virus disease. Perspectives from west africa. Am. J. Respir. Crit. Care Med. *190*, 733–737. https://doi.org/10.1164/rccm.201408-1514cp.

Furuyama, W., and Marzi, A. (2020). Development of an enzyme-linked immunosorbent assay to determine the expression dynamics of ebola virus soluble glycoprotein during infection. Microorganisms *8*, 1535. https://doi.org/10.3390/microorganisms8101535.

Giannetti, A., Barucci, A., Berneschi, S., Cosci, A., Cosi, F., Farnesi, D., Nunzi Conti, G., Pelli, S., Soria, S., Tombelli, S., et al. (2015). Optical micro-bubble resonators as promising biosensors. In Optical Sensors 2015, *9506* (SPIE), pp. 241–247.

Greenbaum, A., Akbari, N., Feizi, A., Luo, W., and Ozcan, A. (2013). Field-portable pixel super-resolution colour microscope. PLoS One *8*, e76475. https://doi.org/10.1371/journal.pone.0076475.

Institute of Medicine Committee on emerging microbial threats to Health (1992). In Emerging Infections: Microbial Threats to Health in the United States, J. Lederberg, R.E. Shope, and S.C. Oaks, eds. (National Academies Press (US)).

Jiang, X., Qavi, A.J., Huang, S.H., and Yang, L. (2020). Whispering-Gallery Sensors. Matter *3*, 371–392. https://doi.org/10.1016/j.matt.2020.07.008.

Jones, K.E., Patel, N.G., Levy, M.A., Storeygard, A., Balk, D., Gittleman, J.L., and Daszak, P. (2008). Global trends in emerging infectious diseases. Nature *451*, 990–993. https://doi.org/10.1038/nature06536.

Kebenei, C.K., and Okoth, P. (2021). Ebola virus disease, diagnostics and therapeutics: where is the consensus in over three decades of clinical Research? Sci. African *13*, e00862. https://doi.org/10.1016/j.sciaf.2021.e00862.

Khan, A.S., Tshioko, F.K., Heymann, D.L., Le Guenno, B., Nabeth, P., Kerstiëns, B., Fleerackers, Y., Kilmarx, P.H., Rodier, G.R., Nkuku, O., et al. (1999). The reemergence of Ebola hemorrhagic fever, Democratic Republic of the Congo, 1995. Commission de Lutte contre les Epidémies à Kikwit. J. Infect. Dis. *179*, S76–S86. https://doi.org/10.1086/514306.

Kindt, J.T., Luchansky, M.S., Qavi, A.J., Lee, S.-H., and Bailey, R.C. (2013). Subpicogram per milliliter detection of interleukins using silicon photonic microring resonators and an enzymatic signal enhancement strategy. Anal. Chem. *85*, 10653–10657. https://doi.org/10.1021/ac402972d.

Kindzelskii, A.L., Yang, Z.y., Nabel, G.J., Todd, R.F., 3rd, and Petty, H.R. (2000). Ebola virus secretory glycoprotein (sGP) diminishes Fc gamma RIIIB-to-CR3 proximity on neutrophils. J. Immunol. *164*, 953–958. https://doi.org/10.4049/jimmunol.164.2.953.

Lau, R., Wang, A., Chong-Kit, A., Ralevski, F., and Boggild, A.K. (2015). Evaluation of Ebola virus inactivation procedures for Plasmodium falciparum malaria diagnostics. J. Clin. Microbiol. *53*, 1387–1390. https://doi.org/10.1128/jcm.00165-15.

Lindblade, K.A., Kateh, F., Nagbe, T.K., Neatherlin, J.C., Pillai, S.K., Attfield, K.R., Dweh, E., Barradas, D.T., Williams, S.G., Blackley, D.J., et al. (2015). Decreased ebola transmission after rapid response to outbreaks in remote areas, Liberia, 2014. Emerg. Infect. Dis. *21*, 1800–1807. https://doi.org/10.3201/eid2110.150912.

McClellan, M.S., Domier, L.L., and Bailey, R.C. (2012). Label-free virus detection using silicon photonic microring resonators. Biosens. Bioelectron. *31*, 388–392. https://doi.org/10.1016/j.bios.2011.10.056.

McLeod, E., Nguyen, C., Huang, P., Luo, W., Veli, M., and Ozcan, A. (2014). Tunable vapor-condensed nanolenses. ACS Nano *8*, 7340–7349. https://doi.org/10.1021/nn502453h.

Medfisch, S.M., Muehl, E.M., Morrissey, J.H., and Bailey, R.C. (2020). Phosphatidylethanolamine-phosphatidylserine binding synergy of seven coagulation factors revealed using Nanodisc arrays on silicon photonic sensors. Sci. Rep. *10*, 17407. https://doi.org/10.1038/s41598-020-73647-3.

Mitchell, S.W., and McCormick, J.B. (1984). Physicochemical inactivation of Lassa, Ebola, and Marburg viruses and effect on clinical laboratory analyses. J. Clin. Microbiol. *20*, 486–489. https://doi.org/10.1128/jcm.20.3.486-489.1984.

Moran, Z., Rodriguez, W., Ahmadou, D., Soropogui, B., Magassouba, N.F., Kelly-Cirino, C., and Ben Amor, Y. (2020). Comparative performance study of three Ebola rapid diagnostic tests in Guinea. BMC Infect. Dis. *20*, 670. https://doi.org/10.1186/s12879-020-05339-2.

Mordan, E.H., Wade, J.H., Pearce, E., Meunier, D.M., and Bailey, R.C. (2020). A linear mass concentration detector for solvent gradient polymer separations. Analyst *145*, 4484–4493. https://doi.org/10.1039/c9an02533b.

Morens, D.M., Folkers, G.K., and Fauci, A.S. (2004). The challenge of emerging and re-emerging infectious diseases. Nature *430*, 242–249. https://doi.org/10.1038/nature02759.

Mudanyali, O., McLeod, E., Luo, W., Greenbaum, A., Coskun, A.F., Hennequin, Y., Allier, C.P., and Ozcan, A. (2013). Wide-field optical detection of nanoparticles using on-chip microscopy and self-assembled nanolenses. Nat. Photonics *7*, 247–254. https://doi.org/10.1038/nphoton.2012.337.

Pallesen, J., Murin, C.D., de Val, N., Cottrell, C.A., Hastie, K.M., Turner, H.L., Fusco, M.L., Flyak, A.I., Zeitlin, L., Crowe, J.E., Jr., et al. (2016). Structures of Ebola virus GP and sGP in complex with therapeutic antibodies. Nat. Microbiol. *1*, 16128. https://doi.org/10.1038/nmicrobiol.2016.128.

Pettitt, J., Zeitlin, L., Kim, D.H., Working, C., Johnson, J.C., Bohorov, O., Bratcher, B., Hiatt, E., Hume, S.D., Johnson, A.K., et al. (2013). Therapeutic intervention of Ebola virus infection in rhesus macaques with the MB-003 monoclonal antibody cocktail. Sci. Transl. Med. *5*, 199ra113. https://doi.org/10.1126/scitranslmed.3006608.

Qavi, A.J., and Bailey, R.C. (2010). Multiplexed detection and label-free quantitation of microRNAs using arrays of silicon photonic microring resonators. Angew. Chem. *49*, 4608–4611. https://doi.org/10.1002/anie.201001712.

Qavi, A.J., Kindt, J.T., Gleeson, M.A., and Bailey, R.C. (2011). Anti-DNA:RNA antibodies and silicon photonic microring resonators: increased sensitivity for multiplexed microRNA detection. Anal. Chem. *83*, 5949–5956. https://doi.org/10.1021/ac201340s.

Robison, H.M., and Bailey, R.C. (2017). A Guide to quantitative biomarker assay development using whispering gallery mode biosensors. Curr. Protoc. Chem. Biol. *9*, 158–173. https://doi.org/10.1002/cpch.23.

Robison, H.M., Chapman, C.A., Zhou, H., Erskine, C.L., Theel, E., Peikert, T., Lindestam Arlehamn, C.S., Sette, A., Bushell, C., Welge, M., et al. (2021). Risk assessment of latent tuberculosis infection through a multiplexed cytokine biosensor assay and machine learning feature selection. Sci. Rep. *11*, 20544. https://doi.org/10.1038/s41598-021-99754-3.

Robison, H.M., Escalante, P., Valera, E., Erskine, C.L., Auvil, L., Sasieta, H.C., Bushell, C., Welge, M., and Bailey, R.C. (2019). Precision immunoprofiling to reveal diagnostic signatures for latent tuberculosis infection and reactivation risk stratification. Integr. Biol. *11*, 16–25. https://doi.org/10.1093/intbio/zyz001.

Rugarabamu, S., Mboera, L., Rweyemamu, M., Mwanyika, G., Lutwama, J., Paweska, J., and Misinzo, G. (2020). Forty-two years of responding to Ebola virus outbreaks in Sub-Saharan Africa: a review. BMJ Glob. Health *5*, e001955. https://doi.org/10.1136/bmjgh-2019-001955.

Sagripanti, J.-L., and Lytle, C.D. (2011). Sensitivity to ultraviolet radiation of Lassa, vaccinia, and Ebola viruses dried on surfaces. Arch. Virol. *156*, 489–494. https://doi.org/10.1007/s00705-010-0847-1.

Sanchez, A., Yang, Z.Y., Xu, L., Nabel, G.J., Crews, T., and Peters, C.J. (1998). Biochemical analysis of the secreted and virion glycoproteins of Ebola virus. J. Virol. *72*, 6442–6447. https://doi.org/10.1128/jvi.72.8.6442-6447.1998.

Scheler, O., Kindt, J.T., Qavi, A.J., Kaplinski, L., Glynn, B., Barry, T., Kurg, A., and Bailey, R.C. (2012). Label-free, multiplexed detection of bacterial tmRNA using silicon photonic microring resonators. Biosens. Bioelectron. *36*, 56–61. https://doi.org/10.1016/j.bios.2012.03.037.

Shia, W.W., and Bailey, R.C. (2013). Single domain antibodies for the detection of ricin using silicon photonic microring resonator arrays. Anal. Chem. *85*, 805–810. https://doi.org/10.1021/ac3030416.

Suter, J.D., White, I.M., Zhu, H., Shi, H., Caldwell, C.W., and Fan, X. (2008). Label-free quantitative DNA detection using the liquid core optical ring resonator. Biosens. Bioelectron. *23*, 1003–1009. https://doi.org/10.1016/j.bios.2007.10.005.

USAMRIID (2016). In Specimen Collection and Submission Manual, D.O. Defense, ed. (USAMRIID).

Volchkova, V.A., Feldmann, H., Klenk, H.D., and Volchkov, V.E. (1998). The nonstructural small glycoprotein sGP of Ebola virus is secreted as an antiparallel-orientated homodimer. Virology *250*, 408–414. https://doi.org/10.1006/viro.1998.9389.

Wade, J.H., Alsop, A.T., Vertin, N.R., Yang, H., Johnson, M.D., and Bailey, R.C. (2015). Rapid, multiplexed phosphoprotein profiling using silicon photonic sensor arrays. ACS Cent. Sci. *1*, 374–382. https://doi.org/10.1021/acscentsci.5b00250.

Wahl-Jensen, V.M., Afanasieva, T.A., Seebach, J., Ströher, U., Feldmann, H., and Schnittler, H.J. (2005). Effects of Ebola virus glycoproteins on endothelial cell activation and barrier function. J. Virol. *79*, 10442–10450. https://doi.org/10.1128/jvi.79.16.10442-10450.2005.

Warfield, K.L., Swenson, D.L., Olinger, G.G., Kalina, W.V., Viard, M., Aitichou, M., Chi, X., Ibrahim, S., Blumenthal, R., Raviv, Y., et al. (2007). Ebola virus inactivation with preservation of antigenic and structural integrity by a photoinducible alkylating agent. J. Infect. Dis. *196*, S276–S283. https://doi.org/10.1086/520605.

Washburn, A.L., Gunn, L.C., and Bailey, R.C. (2009). Label-free quantitation of a cancer biomarker in complex media using silicon photonic microring resonators. Anal. Chem. *81*, 9499–9506. https://doi.org/10.1021/ac902006p.

Wetzler, S.P., Miller, K.A., Kisley, L., Stanton, A.L.D., Braun, P.V., and Bailey, R.C. (2020). Real-time measurement of polymer brush dynamics using silicon photonic microring resonators: analyte partitioning and interior brush kinetics. Langmuir *36*, 10351–10360. https://doi.org/10.1021/acs.langmuir.0c01336.

Woolhouse, M.E., and Gowtage-Sequeria, S. (2005). Host range and emerging and reemerging pathogens. Emerg. Infect. Dis. *11*, 1842–1847. https://doi.org/10.3201/eid1112.050997.

Xu, X., Jiang, X., Zhao, G., and Yang, L. (2016). Phone-sized whispering-gallery microresonator sensing system. Opt Express *24*, 25905–25910. https://doi.org/10.1364/oe.24.025905.

Yu, D., Humar, M., Meserve, K., Bailey, R.C., Chormaic, S.N., and Vollmer, F. (2021). Whispering-gallery-mode sensors for biological and physical sensing. Nat. Rev. Methods Primers *1*, 83. https://doi.org/10.1038/s43586-021-00079-2.

Zhu, H., White, I.M., Suter, J.D., Dale, P.S., and Fan, X. (2007). Analysis of biomolecule detection with optofluidic ring resonator sensors. Opt. Express *15*, 9139–9146. https://doi.org/10.1364/oe.15.009139.

Zhu, W., Banadyga, L., Emeterio, K., Wong, G., and Qiu, X. (2019). The roles of ebola virus soluble glycoprotein in replication, pathogenesis, and countermeasure development. Viruses *11*, 999. https://doi.org/10.3390/v11110999.

STAR★METHODS

KEY RESOURCES TABLE

REAGENT or RESOURCE	SOURCE	IDENTIFIER
Antibodies		
Anti-EBOV capture Ab, desalted, stored at 0.5 mg/mL	Integrated BioTherapeutics	Cat#: 0365-001
Anti-SUDV capture Ab, desalted, stored at 0.5 mg/mL	Integrated BioTherapeutics	Cat#: 0302-030
Biotinylated Anti-EBOV/SUDV pan Ab	Integrated BioTherapeutics	N/A
Ms IgG control Ab, 5 mg/mL	Thermo Fisher Scientific	Cat #: 0031903
Biological samples		
NHP serum: Rhesus macaque	USAMRIID (Pettitt et al., 2013)	N/A
Pooled healthy serum: Human	Innovative Research, Novi, MI	Cat #: ISER50ML
Chemicals, peptides, and recombinant proteins		
Recombinant EBOV Soluble GP (sGP)	Integrated BioTherapeutics	Cat#: 0565-001
Recombinant SUDV Soluble GP (sGP)	Integrated BioTherapeutics	Cat#: 0570-001
Acetone (7.9 mL)	Fisher Chemical	Cat#: A184
Isopropanol (2 mL)	Fisher Chemical	Cat#: A4154
3-aminopropyltriethoxysilane (APTES, 100 μL)	Sigma Aldrich	Cat#: 440140
Bis(sulfosuccinimidyl)suberate (BS3, 2 mg)	Thermo Fisher Scientific	Cat#: A39266
Acetic acid (2 mM)	Fisher Chemical	Cat#: A38-212
Glycerol (50% solution)	Sigma Aldrich	Cat#: G5516
DryCoat Assay Stabilizer	Virusys Corporation	Cat#: AG066-1
Starting Block Buffer	Thermo Fisher Scientific	Cat#: 37578
Streptavidin horseradish peroxidase	Thermo Fisher Scientific	Cat#: 21130
4-chloro-1-napthol (4-CN)	Thermo Fisher Scientific	Cat#: 34012
Software and algorithms		
Genaltye Matchbox User Interface	Genalyte, Inc.	MavII Host 8.2
RStudio: Integrated Development Environment for R	RStudio, Inc.	Version 1.2.5001
Nanodrop1000 User Interface	Thermo Fisher Scientific	Version 3.8.1
Other		
Matchbox Instrument, Maverick Detection System	Genalyte, Inc.	N/A
Unstripped Silicon Photonic Chips	Genalyte, Inc.	N/A
Chip Carriers with Back Door Adhesive	Genalyte, Inc.	N/A
Zeba Sip Desalting Columns, 7K MWCO	Thermo Fisher Scientific	Cat#: 89882
Vortexer	Thermo Fisher Scientific	Cat#: 12-812
Microscope	Leica	Cat#: EZ4W
The Belly Dancer Orbital Shaker	IBI Scientific	Model#: BDRAA115S
Microcentrifuge tubes (0.6 mL)	Thermo Fisher Scientific	Cat#: 02-682-000
Microcentrifuge tubes (1.5 mL)	Thermo Fisher Scientific	Cat#: 02-682-002
Microcentrifuge tubes (5 mL)	Thermo Fisher Scientific	Cat#: 14-282-300
DURX 670, cleanroom wipe	Berkshire	Cat#: DR670.0909.20
24 well plate with lid	Thermo Fisher Scientific	Cat#: 142485
96 well V-bottom plate	Corning	Cat#: 3357
20 mL Glass Screw-Thread Scintillation Vials	Fisher Scientific	Cat#: 03-340-4L
Monoject 1 mL Tuberculin Syringe (Regular Tip)	Fisher Scientific	Cat#: 22-257-135
BD PrecisionGlide Needle, 26G x ½	Thermo Fisher Scientific	Cat#: 14-826-15
Nanodrop1000 Spectrophotometer	Thermo Fisher Scientific	Cat#: ND-1000(US\CAN)

CellPress
OPEN ACCESS

RESOURCE AVAILABILITY

Lead contact

Further information and requests for resources and reagents should be directed to the Lead Contact, Gaya Amarasinghe (gamarasinghe@wustl.edu).

Materials availability

This study did not generate new unique reagents.

Data and code availability

- This study did not generate datasets.
- This paper does not report original code.
- Any additional information required to reanalyze the data reported in this paper is available from the lead contact upon request.

METHOD DETAILS

Capture agents and antigens

Antibodies and antigens used in this study were obtained from Integrated Biotherapeutics (Rockville, MD), except for Mouse IgG (ThermoFisher Scientific, Rockford, Illinois), which served as a binding control.

Photonic microring resonators

Measurements were performed with a Maverick Matchbox optical scanning instrument and silicon sensor chips fabricated by Genalyte, Inc. (San Diego, CA). Experiments were performed on 4 × 6 mm sensor chips containing 128 microring sensors, each 30 μm in diameter, arranged in clusters of four. The clusters are split between two microfluidic channels, with four additional unfunctionalized temperature control rings on each chip.

Chemical functionalization and immobilization of capture antibodies on sensor chips

Antibodies were covalently attached to the microring sensor surfaces as previously described (Robison and Bailey, 2017). Briefly, the chips were silanized with 1% (3-Aminopropyl)triethoxysilane (APTES, Sigma) to add primary amines to the sensor surfaces. The sensors were incubated with 5 mM bis(sulfosuccinimidyl)suberate (BS3, Thermo Fisher Scientific), an amine-reactive, homobifunctional crosslinker, for 3 minutes. The sensor chips were dipped in H_2O to remove unreacted BS3 and dried with N_2. Approximately 0.2 μL of each primary capture antibody diluted to 0.25 mg/mL was spotted onto two to five ring clusters in each of the two channels and incubated for 1 hour. Primary capture antibodies were desalted on Zeba Spin Desalting Columns (7K MWCO, Thermo Fisher Scientific) prior to covalent attachment to the ring surfaces to remove any residual amines that would cross-react with BS3. The sensor chips were blocked using starting block buffer (Thermo Fisher Scientific) for 1 hour, dried with N2 and coated with DryCoat Assay Stabilizer (Virusys Corporation) for storage in a 4°C humidity chamber until use.

Assay set-up

Functionalized chips were housed in a disposable, injection molded, two-channel microfluidic cartridge and inset into the instrument. All fluidic handling was controlled at a flow rate of 30 μL/min via a series of pumps. Due to the two-channel microfluidic design, two assays were simultaneously completed on one chip. For immunoassay analysis, running buffer (1X phosphate buffered saline, PBS, Sigma) with 0.5% bovine serum albumin (BSA, Sigma) was first flowed across the channel surface for at least 5 minutes to equilibrate the system prior to analysis. Assay steps for each experiment were as follows: running buffer (2 min), sample (7 min), running buffer (2 min), biotinylated tracer antibody (2 μg/mL, 7 min), running buffer (2 min), streptavidin- horseradish peroxidase (3 μg/mL, SAHRP, Thermo Fisher Scientific) (7 min), running buffer (2 min), 4-chloro-1-napthol (4-CN, Thermo Fisher scientific) (7 min), running buffer (2 min).

Calibrations and sample analysis

Immunoassays for EBOV sGP and Sudan ebolavirus (SUDV) sGP were simultaneously calibrated in parallel. Serial dilutions of antigen from a saturating concentration to an undetectable concentration resulted in an eight-point calibration curve for each target. Calibrations were constructed in 1%, 10%, and 50% serum matrices. Samples were diluted and analyzed at 10X or 100X, allowing the concentrations to remain in the quantitative regime of the calibration curves.

NHP sera samples

The kinetics of sGP production *in vivo* was tested in rhesus macaques challenged with 1,000 PFU of EBOV and treated post exposure with either a cocktail of three monoclonal antibodies (MB-03) (Pettitt et al., 2013) or vehicle control. Longitudinal serum samples on days 0-15, 21, and 28 from survivors and days 0 through the day of death for fatal cases were prepared and tested by our quantitative sGP ELISA content and by PCR for EBOV genome content. Samples were stored at −80°C until use in this study.

All of these animal studies were performed under approval of the local IACUC committees. All work was performed in compliance with the Animal Welfare Act and other federal statutes and regulations relating to animals. The USARMIID is accredited by the Association for Assessment and Accreditation of Laboratory Animal Care, International (AAALAC) and adhere to principles stated in the Guide for the Care and Use of Laboratory Animals, National Research Council. All challenge studies were conducted under maximum containment in an animal biosafety level (BSL)-4 facility at USAMRIID.

ELISAs

A quantitative ELISA to detect sGP resulting from virus infection was developed in-house at Integrated Biotherapeutics. Critical reagents were generated to support the development of the ELISA. Specifically, a recombinant sGP was developed in-house at Integrated Biotherapeutics in order to standardize the quantitation of sGP levels in serum samples. A capture antibody was generated that specifically recognizes EBOV sGP and not the full-length GP. A number of secondary antibodies were evaluated and one monoclonal antibody was selected for use in this assay. Using these reagents, an ELISA method was developed and optimized for reproducibility and robustness. sGP as early as day 3 post challenge was detected in NHPs. Also, the level of sGP in the serum appears to correlate with survival, similar to what is observed in the viremia results as determined by RT-PCR.

PCR

Blood samples were processed for qRT-PCR. USAMRIID standard procedure were used to process the serum samples and determine serum viremia levels (USAMRIID, 2016).

QUANTIFICATION AND STATISTICAL ANALYSIS

Microring resonator data analysis

Analysis of data was performed using an in-house developed R-script as previously described (Robison and Bailey, 2017), but could be completed using standard excel software functions. Briefly, resonance shifts from each individual sensor were tracked over the course of the experiment and the net shift of resonant wavelength of each sensor ring before and after the 4-CN amplification step were analyzed. The net shift of all rings spotted with a specific antibody was averaged across each channel for each experiment. The average net shift was used to calculate the target concentration in each sample based on the appropriate calibration curve fit (e.g., 1% serum calibration for 100X dilution and 10% serum calibration for 10X dilutions). If two dilutions of the same sample were performed, the dilution that resulted in a net shift closest to the inflection point of the respective calibration curve was selected for use.